Appl. Phys. B (2014) 115:263–268
DOI 10.1007/s00340-013-5599-7

Applied Physics B
Lasers and Optics

Ultra-compact TDLAS humidity measurement cell with advanced signal processing

A. Hartmann · R. Strzoda · R. Schrobenhauser · R. Weigel

Received: 13 March 2013 / Accepted: 24 July 2013 / Published online: 1 August 2013

Abstract In this paper, tunable diode laser absorption spectroscopy humidity measurements with an ultra-compact measurement cell are presented. The optical path length is 2 cm. The system uses a vertical cavity surface emitting laser at 1.854 μm. The main limiting factor of the humidity resolution is not the noise but interference fringes produced by reflecting surfaces. Next to the system setup, a novel rejection method to eliminate these fringes, based on Fourier domain analysis of the absorption line, is described. In contrast to other fringe rejection methods, the presented method is able to handle fringes, whose free spectral range is in the range of the half width of the absorption line. The achievable humidity resolution for the presented cell is below 0.25 % relative humidity at room temperature.

1 Introduction

Tunable diode laser absorption spectroscopy (TDLAS) is a powerful technique for the measurement of different gases. Next to scientific trace gas measurements, it is used more and more in industrial and other areas. The analysis of the exhaust in burning processes [1] and the analysis of biomarkers in exhaled air [2] for medical diagnostics are only two examples of a variety of possible applications. Lifetime stability, high sensitivity and a high gas selectivity are the main advantages of TDLAS compared to other gas detection systems. The required size of the optical gas cell, however, is a great disadvantage for compact laser sensor-based systems. Humidity measurement is an important technique in many different fields.

Correct humidity values are essential in dehydration processes, food storage and are in combination with carbon dioxide measurements very important for smart air conditioning. The strong water vapor absorption lines around 1.854 μm in combination with a VCSEL emitting its light in this wavelength range enable not only trace gas measurements with long path cells but also the reduction in the optical path length for ambient humidity measurements. With a 2 cm cell, the strongest absorption line in this region absorbs almost 6 % of the light at a concentration of 1.5 vol%. Figure 1 illustrates a part of the water vapor spectrum from 1.85 to 1.86 μm, calculated by means of HITRAN data [3].

Using an optical path length in the range of a few centimeters, the main limiting factor for the system resolution is not the system noise but interference fringes generated by parallel reflecting surfaces. Of course there is a goal in designing the cell that no direct parallel surfaces occur, but for such short cells, there is often no practical way to eliminate the fringes completely, especially if the cell is in a compact housing. The literature describes several different ways to handle interference fringes. A common way is the use of mechanical modulation of optical elements. Doing this, the fringe modulation phase changes constantly. An integration of the signal eliminates the fringe. This method is very effective but increases the system complexity and reduces the measurement rate. There are also several filtering techniques described, but

A. Hartmann (✉) · R. Strzoda · R. Schrobenhauser
Siemens AG, Corporate Technology, Otto-Hahn-Ring 6,
81739 Munich, Germany
e-mail: HartmannAl@gmx.de;
Hartmann.Alexander.ext@siemens.com

A. Hartmann · R. Weigel
Institute for Electronics Engineering,
University of Erlangen-Nuremberg, Cauerstrasse 9,
91058 Erlangen, Germany

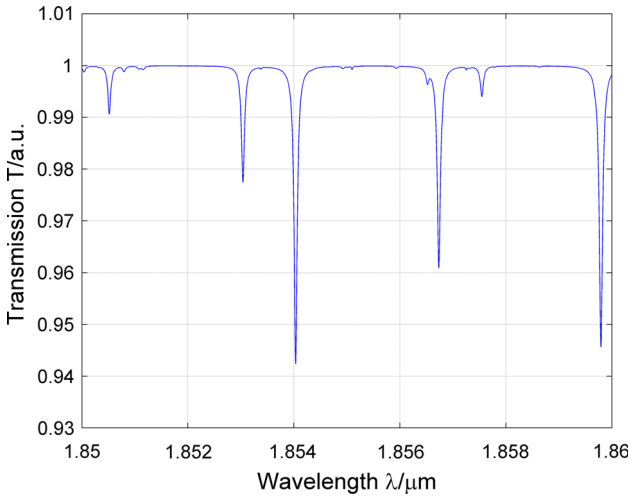

Fig. 1 Humidity spectrum around 1.854 μm, water vapor concentration 1.5 vol %, path length 2 cm

each approach has its problems with fringes whose free spectral range (FSR) is in the range of the absorption line width. Hodgkinson and Tatam [4] give a general summary about the different fringe rejection techniques.

In the following section, the design of the optical cell is presented, and the occurring light reflections are illustrated. Section 3 describes the theory of the signal in time and Fourier domain. Afterward, the interference elimination method as well as the window stabilization is pointed out. Section 6 discusses the results and the advantage of the fringe elimination technique on a basic curve fit.

2 Design of the optical cell

The humidity cell is illustrated in Fig. 2, top. Through a 20 × 10 × 10 mm cuboid, a hole of 8.5 mm diameter as optical cell is drilled. Perpendicular to this, there is a second, rectangular hole for gas exchange. The VCSEL chip[1] emits its light at 1,854 ± 2 nm through an angled window. The beam divergence is specified to 10°–25° by the manufacturer. To maintain simplicity and to avoid a reflection of a focused beam, no lenses are used. The laser (blue) is fixed in the cell with a screwed panel. For the photo diode[2] (green), an angular mount was milled. Caused by the immersion depth of laser and photo diode in the cube, an optical cell length of exactly 2 cm is achieved. The schematic in Fig. 2 bottom illustrates the light path between laser diode and photo diode. A part of the beam is absorbed at the photo diode; the other part is reflected by different components. In a cell with such a short length, a

[1] TO-46 housing, VERTILAS GmbH http://www.vertilas.de.

[2] TO-18 housing, Teledyne Judson Technologies http://www.judsontechnologies.com.

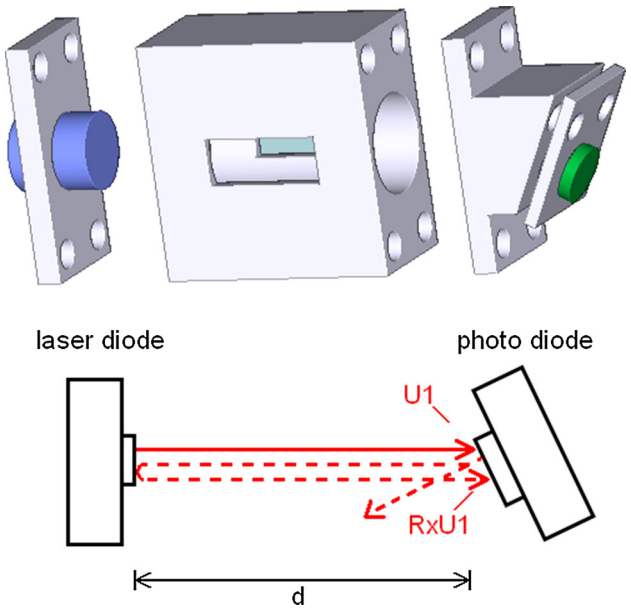

Fig. 2 *Top* humidity measurement probe with laser (*blue*) and photo diode (*green*); *bottom* schematic of the cell with U1 the initial and RxU1 the additional, reflected beam

multiple reflection of a part of the light between laser and photo diode is nearly unavoidable. In the picture, this is denoted by a reflection factor R multiplied with the initial beam $U1$.

3 Signal

Figure 3, top indicates the received signal at the photo diode. The laser is tuned by its current over the absorption line at 1.854 μm. Figure 3, bottom shows the signal without the laser background. The occurring interference modulation could easily assign to the cell length by means of the FSR. The figure shows two conditions of the signal. The gas absorption is in both cases the same, but the interference fringe changed in its phase relative to the absorption line. This movement is due to very small changes in the resonator length d, already caused by small ambient temperature changes. The signal without laser background is in principle described as follows.

Time domain The absorption of light in gas is defined by Beer–Lambert law [5]:

$$T(\lambda) = I(\lambda)/I_0 = \exp(-\alpha(\lambda) \cdot c \cdot l) \quad (1)$$

with T the light transmission, I the received and I_0 the initial light intensity, λ the wavelength, l and c the cell length and gas concentration. Simplified, the wavelength-dependent absorption coefficient $\alpha(\lambda)$ is a Lorentzian-shaped signal for room conditions, and the Gaussian part of the shape is neglected. It could be calculated with

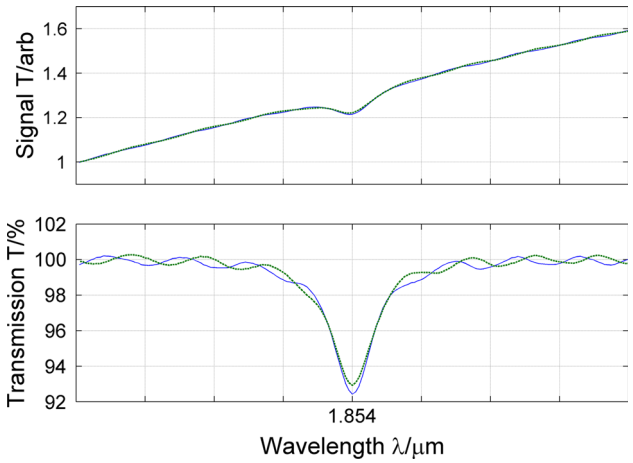

Fig. 3 *Top* absorption line on laser background; *bottom* absorption line without background, interference fringes observable

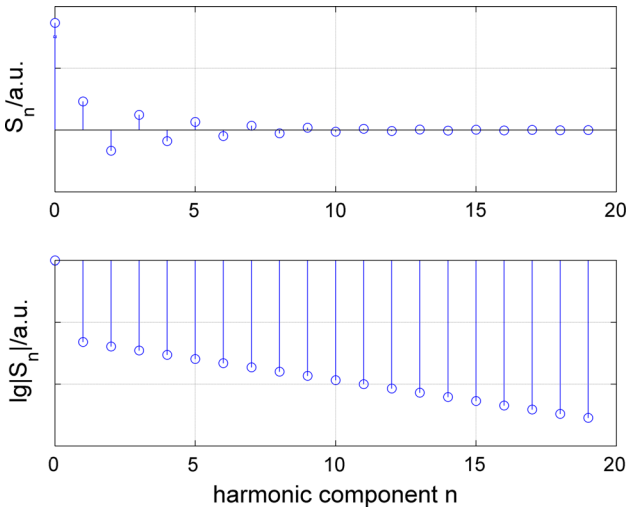

Fig. 4 *Top* first components of the harmonic spectrum of the absorption line; *bottom* components of harmonic spectrum form a decreasing line in logarithmic scale

$$\alpha(\lambda) \approx S/(1 + ((\lambda - \lambda_0)/\gamma_L)^2) \tag{2}$$

S denotes the line strength, λ_0 the line center and γ_L the Lorentzian line width.

The laser light intensity including an interference fringe is described with following equation [6].

$$T(\lambda) = 1/(1 + |r|^2 - 2|r|\cos(2\pi/\mathrm{FSR} \cdot \lambda + \phi)) \tag{3}$$

with r the reflection factor and ϕ the phase shift of the interference fringe. For small r, this equation can be approximated:

$$T(\lambda) \approx (1 + A\cos(2\pi/\mathrm{FSR} \cdot \lambda + \phi)) \tag{4}$$

A denotes the fringe amplitude. Furthermore, if r is small, i.e., the amplitude of the fringe modulation is small on the background, the additional absorption of the light caused by multiple reflections is negligible. Therefore, the transmission including absorption line and fringe could be approximated by the summation of the two parts (Eq. 5).

$$T(\lambda) \approx [\exp(-\alpha(\lambda) \cdot c \cdot l) + A\cos(2\pi/\mathrm{FSR} \cdot \lambda + \phi)] \tag{5}$$

Fourier domain By calculating the discrete Fourier transform (DFT), the signal is transformed to the Fourier domain. The harmonic spectrum of the absorption signal in itself decreases in an exponential form with alternating sign (Fig. 4, top). In logarithmic scale, the absolute values of the harmonics form a decreasing straight trend (Fig. 4, bottom).

Arndt [7] calculated an analytical expression for the harmonic components of a Lorentzian signal broadened by modulation. The special case for the modulated line center ($\lambda_0 = 0$) is listed in Eq. (6). Equation (7) illustrates the straight trend of the Fourier amplitudes in logarithmic form on the harmonic n:

$$\begin{aligned} &|S_n(\lambda_0 = 0, m)| \\ &\quad = |2S/\mathrm{sqrt}(1 + m/\gamma_\mathrm{L})^2 \cdot (\mathrm{sqrt}(1 + (m/\gamma_\mathrm{L})^2) \\ &\quad - 1)^n/(m/\gamma_\mathrm{L})^n| \end{aligned} \tag{6}$$

$$\begin{aligned} &\log10|S_n(\lambda_0 = 0, m)| \\ &\quad = \log10|2S/\mathrm{sqrt}(1 + m/\gamma_\mathrm{L})^2| + n \\ &\quad \cdot \log10|(\mathrm{sqrt}(1 + (m/\gamma_\mathrm{L})^2) - 1)/(m/\gamma_\mathrm{L})| \end{aligned} \tag{7}$$

S_n denotes the value and n the number of the harmonic, λ_0 the absorption line center, γ_L the line width and m the width of the measurement range around the absorption line. Log10 is the logarithm on base 10.

Due to the sinusoidal form of the fringe modulation (small amplitude), the interference is a single isolated peak in the discrete Fourier spectrum, if the measurement window is exactly a multiple of the FSR. If the fringe form deviates from the pure sine (see time domain description), the spectrum contains also values on multiples of the fundamental component. For the following basic description of the elimination technique, it is assumed that the signal is a pure sinusoidal one.

4 Elimination method

The spectrum of the signal including absorption line and interference fringe (Fig. 3, bottom) is illustrated in Fig. 5 (circles).

If the size of the measurement window is exactly a multiple of the fringe FSR, the spectrum in logarithmic scale shows one single deviation from the decreasing straight trend. Now it is possible to interpolate this single

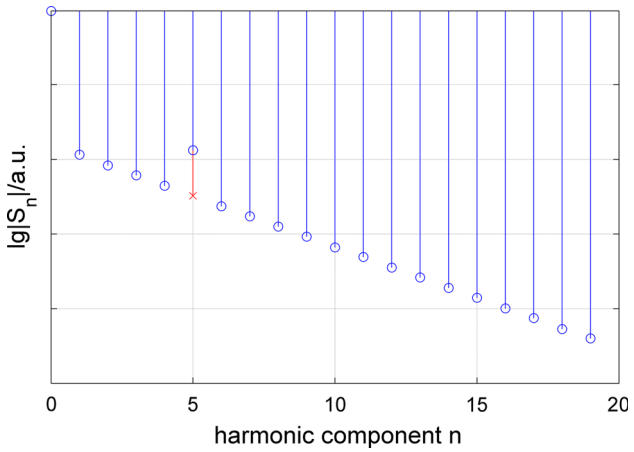

Fig. 5 Fourier spectrum of absorption signal including interference fringes (*circles*), interpolated harmonic (*cross*)

defect (Fig. 5, cross) and to reconstruct the absorption line without interference fringe by using the theory of Fourier series adjusted to the laser spectroscopic signal:

$$T(\lambda) = \sum_{0}^{n} (-1)^n |S_n| \cos(n \cdot 2\pi \cdot (\lambda - \lambda_0)/\Delta\lambda) \tag{8}$$

with $\Delta\lambda$ the size of the measurement window. Afterward, the reconstructed signal is evaluated with a least-squares curve fit.

If the interference modulation deviates from a pure sinusoidal signal, the harmonic components on a multiple of the base modulation, especially twice and three times, could also be interpolated.

The used VCSEL needs a very wide current interval to tune the signal as shown in Fig. 3. Subsequently, also a high difference in received power occurs (approx. 46 %). The absorption line is negligible affected by this difference because it is in the middle of the signal. The amplitude of the fringe, however, is clearly higher at the end as in the beginning of the scanned signal. A direct analysis of the signal without normalizing to the received power would deform the Fourier spectrum of the fringe. Therefore, it is necessary to normalize to the background before analyzing.

5 Window stabilization

As described in the section before, the width of the measurement window must be an exact multiple of the fringe FSR. Next to this, also the absorption line has to be in the center of the measurement window to get a decreasing trend of the harmonics in the Fourier domain. This is ensured by the subtraction of the measured signal with a reversed version of itself:

$$T_{\text{diff}}[n] = T[n] - T[N - n - 1] \tag{9}$$

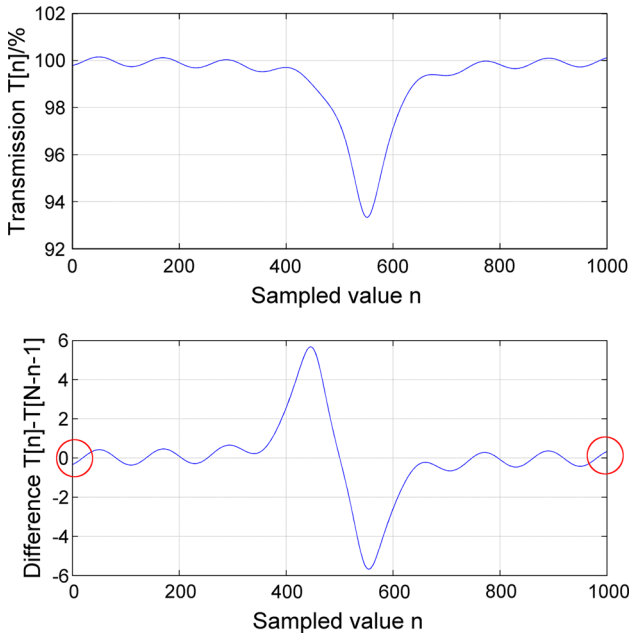

Fig. 6 *Top* signal shifted out of the center, measurement window not exactly a multiple of FSR; *bottom* subtraction of signal and its reversed version

with $T[n]$ the sampled transmission value, $T_{\text{diff}}[n]$ the subtraction value of the signal and its reversed version, n the number of the sampled value and N the total number of sampled values.

Figure 6, top shows a measured signal, where the width of the measurement window is not exactly a multiple of the fringe FSR. Furthermore, the absorption line is not in the center of the window. The subtraction of the signal with its reversed version (further referred as subtraction signal) is plotted in Fig. 6, bottom. If the window width is a multiple of the fringe period, the values of the signal at both ends (n: = {0, 1,000}) are approximately equal; therefore, both ends of the subtraction signal must be zero. If the window width is not exactly, these values are not zero (red circles). A shift of the absorption line out of the center results in a positive and a negative amplitude in the middle of the subtraction signal. The higher the shift of the absorption signal, the larger the positive and negative amplitude. These two indicators enable the system to correct a wrong measurement window width and window shift and therefore to stabilize the signal with respect to optimal fringe rejection.

6 Experimental setup and results

Figure 7, top shows a measured signal of the cell in Fig. 2 with two conditions of the interference fringe. The fringe was forced to move in the measured signal by applying a

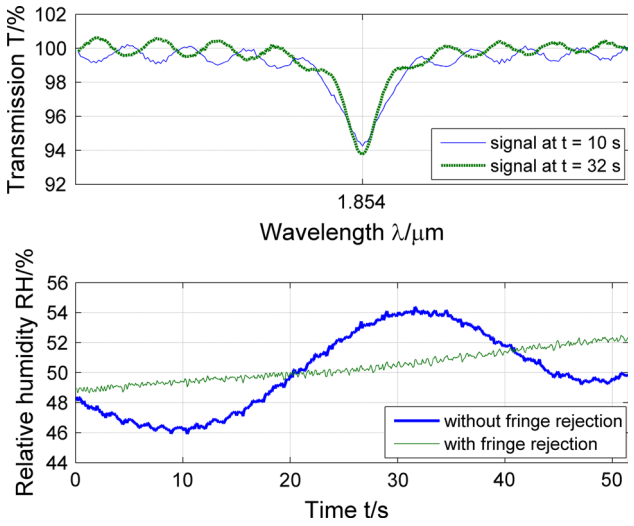

Fig. 7 *Top* interfered signal for 2 cm cell; *bottom* relative humidity concentration at 24 °C, calculated without (*bold line*) and with (*thin line*) fringe rejection

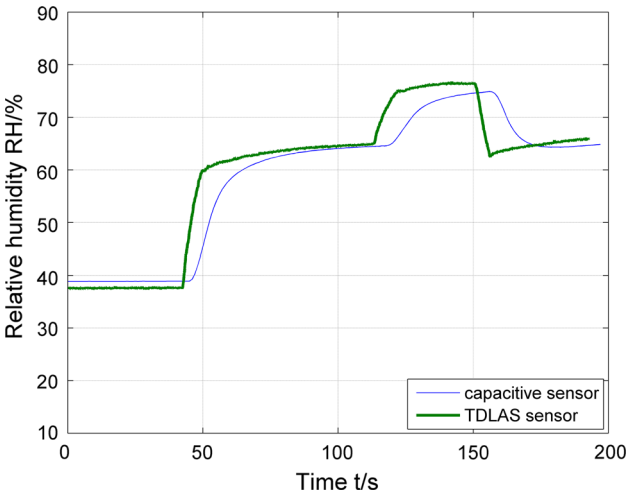

Fig. 8 Comparison of humidity values of a capacitive (*thin line*) and the presented TDLAS sensor (*bold line*)

low power heat source to the probe. Figure 7, bottom is the evaluated relative humidity at 24 °C. The bold line shows the evaluation with a least-squares curve fit, only including the absorption line, not the fringe, in the fit model. The inaccurate concentration modulation caused by the fringe is about 6.5 % (peak to peak) relative humidity (0.7 % absorption). The thin line is evaluated including the presented fringe reduction method. A significant improvement of the signal concentration is reached. The inaccuracy is about 0.2 % (peak to peak) relative humidity (0.021 % absorption). The reasons for the remaining inaccuracy could be found in the influence of peripheral, overlapping fringes with a bit differing FSR. Also, the higher absorption of the multiple reflected light is neglected by this method.

Figure 8 shows a humidity value comparison of a commercial capacitive sensor with the presented TDLAS humidity sensor. The laser-based sensor shows a faster response to changing humidity, only limited by the duration of the gas exchange. Therefore, it is more suitable for applications with rapid changing humidity.

For both experiments, the humidity cell was equipped with a VCSEL, type VL-1854-1, manufactured by VERTILAS GmbH and an InGaAs detector from Teledyne Judson Technologies with a cutoff wavelength of 2.2 μm. The laser control and the analysis of the photo signal were done with a self-made sensor electronics. For the comparison, a capacitive sensor of type SHT71 supplied by Sensirion AG[3] was used. Both sensors were put into an airtight box with gas inlets and an included inside air ventilation for a quick circulation of the inserted gas. The different humidity steps were generated by exhaling into the box.

The presented fringe rejection method is most powerful, when the signal includes one dominating interference fringe. In this case, it is able to reduce the influence of the basic modulation and all overtones with the advantage of avoiding moving parts in the system and long integration times. Therefore, a fast response could be achieved. Theoretically, it is also suited for more than one dominating fringe, when using a window wide, which is the least common multiple of both fringe FSRs. However, in this case, the window width possibly becomes very wide. For systems with a mix of several fringes with different FSRs, e.g., multimode fibers [8], the method is not suitable.

7 Conclusion

By using a vertical cavity surface emitting laser with a wavelength of 1.854 microns, it is possible to reduce the optical path length for ambient humidity measurement down to 2 cm. Due to unavoidable reflections in such a short optical cell, the main limiting factor for the resolution is interference fringes. The presented fringe rejection method is able to reduce the effect of the interference on the humidity values for this cell by a factor of 30. In comparison with other fringe rejection methods, this method is able to handle interference fringes whose FSR is comparable to the absorption line width and does not need moving parts in the setup. Furthermore, a simple technique to handle a change in the ratio of measurement window wide to fringe FSR and signal drifts was developed.

The reduced size of the cell and the overall simplicity of the measurement probe enables the optical sensor to compete with other sensor types, e.g., capacitive ones, with

[3] http://www.sensirion.com.

respect to the probe size but offers faster response time. In addition, it provides lifetime stability which is typical for well-developed TDLAS sensors. The presented humidity measurement is only one example for a compact gas probe, and the signal evaluation is directly transferable to other gases.

References

1. J. Chen, A. Hangauer, R. Strzoda, M.-C. Amann, Appl. Phys. B **100**, 2 (2010)
2. C. Wang, S. Peeyush, Sensors **9**, 10 (2009)
3. L. Rothman, D. Jacuemart, A. Barbe, D.C. Benner, M. Birk, L. Brown, M. Carleer, J. C. Chackerian, K. Chance, L. Coudert, V. Dana, V. Devi, J.-M. Flaud, R. Gamache, A. Goldman, J.-M. Hartmann, K. Jucks, A. Maki, J.-Y. Mandin, S. Massie, J. Orphal, A. Perrin, C. Rinsland, M. Smith, J. Tennyson, R. Tochenov, R. Toth, J.V. Auwera, P. Varanasi, G. Wagner, The HITRAN 2004 molecular spectroscopic database. J. Quan. Spectrosc. Radiat. Transf. **96**, 139–204 (2005)
4. J. Hodgkinson, R.P. Tatam, Meas. Sci. Technol. **24**, 1 (2013)
5. W. Demtroeder, *Laserspektroskopie*, vol. 5 (Springer, Berlin, Heidelberg, 2007)
6. B.E.A. Saleh, M.C. Teich, *Grundlagen der Photonik* (WILEY-VCH, Weinheim, 2008)
7. R. Arndt, J. Appl. Phys. **36**, 2522–2524 (1965)
8. J. Chen, A. Hangauer, R. Strzoda, M. Fleischer, M.-C. Amann, Opt. Lett. **35**, 3577–3579 (2010)